International Forum on Aeroelasticity and Structural Dynamics
IFASD 2017
25-28 June 2017, Como - Italy

# HIGH FIDELITY TRIM CALCULATION UNDER CONSIDERATION OF AEROELASTIC EFFECTS OF A HIGH ASPECT RATIO SWEPT WING

**Andreas Hermanutz[1] and Mirko Hornung[2]**

[1] Technische Universität München,
Chair of Lightweight Structures
andreas.hermanutz@tum.de

[2] Technische Universität München,
Chair of Aircraft Design
mirko.hornung@tum.de

**Keywords:** Computational Fluid Structure Interaction, High Aspect Ratio Wings, Structural Wing Design

**Abstract: New structural wing technologies like morphing structures, high aspect ratio wings or passive as well as active load elevation techniques have in common that flexibility is increasing within the next generation of aircraft wings. Therefore, the aeroelastic effects will rise and sophisticated methods are needed to develop and predict the aircrafts properties, load and overall behavior on a highly accurate level. The presented paper shows the work on virtual aircraft models and the application of high fidelity computational fluid structure interaction methods for the development of structural wing design on a high aspect ratio composite wing transport aircraft demonstrator.**

## 1 INTRODUCTION

Aircraft structures are inherently flexible, and thus deform under loads. If the loads are caused by aerodynamic forces, which themselves dependent on the deformed geometry, an interaction between the structure and the surrounding airflow occurs. These effects described by structural elasticity and aerodynamic forces are known as aeroelasticity. The intensity of the interaction strongly depends on the structural stiffness and the magnitude of aerodynamic forces. Aircraft wings are therefore typical examples for a strongly coupled aeroelastic problem.
In structural aircraft design, reduction mass is one of the major objectives to enable additional payload or fuel. One side effect is, that lowering structural weight leads in general to an increased structural flexibility. Furthermore, to gain the aerodynamic efficiency of modern wings there is the target to establish high aspect ratio (AR) wings in commercial transport aircrafts. An increased AR, and therefore additional wing span needs additional wing stiffness to sustain the aerodynamic loading and increases undesired the structural weight undesirably. Materials like carbon composites are perfect to partially avoid this conflictive situation, due to their high specific stiffness and their anisotropic nature by enabling tailoring capabilities. These effects are used for passive load elevation and are therefore a reasonable way to avoid the additional airframe weight. Together, both design goals are resulting in more flexible wings and therefore to increasing aeroelastic difficulties.

Aircraft loads and the corresponding structural design are important disciplines and play a major role during the entire development process. The described rising interaction between aerodynamics and structural mechanics necessitates an accurate prediction for a successful and improved design. Especially at the conceptual aircraft development design stage, rare knowledge is the reason why fast methods are used to perform extensive parameter studies. Within the further propagating development process, the level of detail is raising and in return, the fidelity of the applied models have to be improved in the same manner. Especially on the aerodynamic side, the great advantage of state-of-the-art potential flow aerodynamic models, which feature a low computational effort for fluid structure interaction, is diminished by the model fidelity. The consideration of 3d flow effects, turbulence, boundary layer influence and the flow conditions in the transonic flight regime are coming into focus. Especially for very flexible wings, high fidelity methods become more important in an earlier design stage, compared to classical wings. A virtual aircraft, which allows accurate prediction of the behavior not only for final design verifications, but also for the detailed design process, is in focus of the presented work.

To evaluate the external aerodynamic load distribution, drag and internal structural loading, quasi-steady equilibrium maneuver flights are used as basic load conditions. The aircraft is trimmed in a flight state, where the aircrafts resulting equilibrium forces are zero. For a given flight maneuver like pull-up or pull-down, aircraft acceleration, counteracting lift and control surfaces are used for aircraft maneuvering. The following work presents the development of a high fidelity CSM-CFD based fluid structure interaction simulation, to perform quasi-steady equilibrium manoeuvers for structural sizing and evaluation of aerodynamic load distribution. The goal is to provide a method with high accuracy and confident results in wing loading, flight shape and aerodynamic efficiency.

## 2 FUNDAMENTALS OF COMPUTATIONAL FLUID STRUCTURE INTERACTION SIMULATION

Fluid Structure Interaction (FSI) is a class of problems with weak or strong dependencies between fluid and structural mechanics. The solution of the flow field depends on the shape of the structure and its motion, and the motion as well as elastic deformation is vise versa influenced by the acting fluidic forces. The inherently non-linear and time depending FSI problems like flexible wings in a flow makes it difficult to find analytical solutions. Therefore, different computational methods have developed over the last years for specific kind of problems.

For both fields, structural mechanics as well as for fluid dynamics, different computational methods are developed and established in aerospace engineering to solve the individual governing equations. To solve the coupled field problems, two main classes of methods, monolithic and staggered coupling, are available. For the presented work, a staggered solution method is used, with the advantage to use the specific knowledge in CSM and CFD for the application in aircraft structural development.

### 2.1 Governing Equation of Computational Mechanics

The structural equilibrium is based on continuums mechanics described in Lagrange formulation by the governing equation (1). Here, $\bar{\bar{S}}$ represents the 2$^{nd}$ Piola-Kirchhoff stress tensor and $\bar{\bar{F}}$ the deformation gradient in material coordinates. Furthermore, $\bar{b}$ is the volume force vector with material density $\rho$ and $\bar{u}$ the structural displacement field.

$$div(\bar{\bar{F}} \cdot \bar{\bar{S}}) + \rho \bar{b} = \rho \frac{\partial^2}{\partial t^2} \bar{u} \tag{1}$$

As numerical method, the Finite Element Method (FEM) is used to obtain a solution for the displacement field $\bar{u}$. Assembling the governing equations for each element results for the general case in a non-linear system of equations as defined in equation (2).

$$K(\bar{u}, \bar{F}) \cdot \bar{u} = \bar{F} \tag{2}$$

For the presented work of a highly flexible wing, major sources for structural non-linearities are large displacements and rotations. Beside the kinematic nonlinearities, also the change of surface normal directions has to be taken into account, resulting in a change of the acting force direction. To consider all these effects, an incremental, implicit solution method as implemented in most commercial FE solvers is used to solve the system of equations.

The fundamental equations of motion for flow problems are described by the Navier-Stoke equations (3). Because not all turbulence cascades are resolved, the formulation as Reynold-Average-Navier Stokes equations are used in combination with an eddy viscosity turbulence model.

$$\begin{gathered} \frac{\partial \rho}{\partial t} + div(\rho \underline{v}) = 0 \\ \frac{\partial(\rho \underline{v})}{\partial t} + div(\rho \underline{v}\, \underline{v}) = -grad(P) + div(\underline{\tau}) + \rho\, \underline{F_v} \\ \frac{\partial(\rho E)}{\partial t} + div(\rho \underline{v}\, E) + div(\underline{v}\, P) = 0 \end{gathered} \tag{3}$$

To solve the non-linear system of equations, a Finite Volume (FV) based discretization is used.

## 2.2 FSI Interface Treatment

Different discretization schemes and resolutions are used for CSM and CFD. That is why the interface between the individual grids are in general non-confirming and for aerospace applications even non-matching. Hence, to transfer the interface variables a mapping method has to be defined. In case of an elastic wing, the variables are the node displacement vector $\bar{u}_I$ and aerodynamic force vector $\bar{F}_I$. Therefore, on structural side wetted, surface elements are defined, which are aligned with the structural shell elements of the skin. The wetted elements use the same shape functions as the undelaying structural elements for the displacement field. Together with a node projection vector for every CFD node, the mapping matrix $\bar{A}$ as defined in equation (4) can be computed.

$$\bar{u}_{CFD} = \bar{A} \cdot \bar{u}_{CSM} \tag{4}$$

The matrix transfers structural displacement to the CFD nodes by a bilinear mapping, based on the linear structural shape functions. This method is known as inverse shape mapping as presented by Farhat [1, 3]. The force transfer in opposite direction of the interface is defined by equation (6). Compared to the displacement mapping, the force transfer has to be conservative in the sense, that no loss or artificial work is produced on the interface. Different possibilities are available to force this requirement as e.g. shown in [2, 3]. In the presented case, the mapping is controlled by the node projection vector from CFD to CSM. The transferred work on each interface side is checked during the simulation as defined by the scalar product in equation (5).

$$\bar{u}_{CFD} \cdot \bar{F}_{CFD} = \bar{u}_{CSM} \cdot \bar{F}_{CSM} \tag{5}$$

In addition, it has to be considered that the FV method is using a cell centered formulation, while the FE formulation uses a node force definition. Therefore an additional mapping matrix $\bar{E}$, which transfers the pressure force to node forces are used. The load transformation is defined in away, that the resulting moment of each element around its center is zero. With the additional constraint, that the applied force $f_i$ on each node should reach a minimum, computing $\bar{E}$ leads to an optimization task, which can be solved analytically as a least square problem.

$$\bar{F}_{CSM} = \bar{A}^T \cdot \bar{E} \cdot \bar{F}_{CFD} \tag{6}$$

Calculating $\bar{A}$ and $\bar{E}$ can computationally be expensive for large problems. Therefore, this is implemented as program in C++ with the capability for parallel execution. Because in structural sizing there are usually no topological changes in the interface mesh, the matrix has to be computed only once at the beginning of the design study.

### 2.3 FSI Coupling Method

The coupling algorithm used for the presented work is mainly motivated by using solvers for CSM and CFD which are highly optimized for the specific physical problems and as well for the numerical solution methods. Furthermore, developing aircraft structures always includes the consideration of different teams working on different topics. Especially in case for the aerodynamic developments the models from aerodynamicist can be reused. Latter one requires that the simulation tools of each single field are used and adapted individually for FSI application. Because of this, the preferred method is a staggered coupling solution. Swept wings are influenced by the wash-out effect when it comes to wing bending. So the coupling method has to be able to consider this strong interaction. An implicit solution method is used with the basic workflow as sketched in Figure 1. This basic algorithm can be characterized as a fix-point iteration and is also extendible to transient problems as shown in [3].

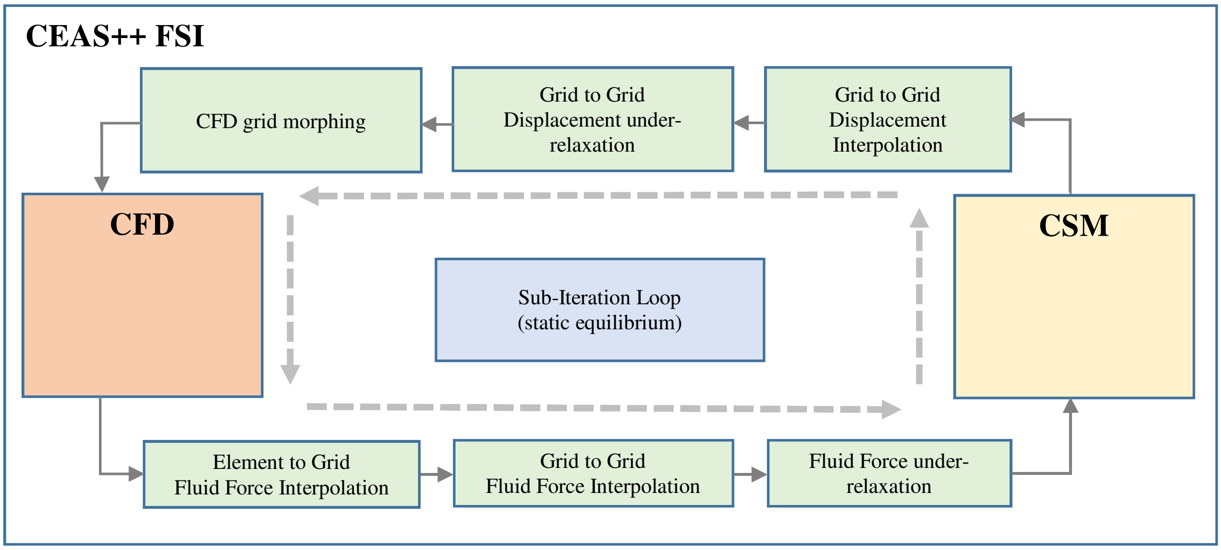


Figure 1: FSI staggered coupling work flow

To stabilize the FSI coupling iterations, the interface variables are getting under-relaxed in the form as shown in equation (7). The under-relaxation parameter $\lambda$ can be defined to be constant or variable like in the Aiken-Method. In the application, only in simple cases a variable $\lambda$ could achieve a significant convergence speed up.

$$x^{i+1} = \lambda x^i + (1 - \lambda)\tilde{x}^{i+1} \tag{7}$$

As already pointed out, the CFD domain features no topological cell changed during the simulation run, but due to the deforming interface the interior domain cells have to be tracked. A local re-meshing would give an adapted mesh to the new interface shape, but it would be computational ineffective, as the CSM-CFD node mapping matrix has to be determined again. It is more effective to track the CFD node by a numerical scheme. For this a mesh morphing based on the diffusion equation (8) is used with the displacement boundary condition defined by the interface.

$$\nabla \cdot \left(\mu \cdot \bar{u}_{CFD,Interior}\right) = 0 \tag{8}$$

The scalar constant parameter $\mu$ is used to control the displacement values close to the interface and the domain far-field. Therefore, $\mu$ is defined as function of the distance to the FSI interface.

As already mentioned, an implicit solution method is performed. So the coupling iterations from Figure 1 are executed several times until convergence occurs. The requirements for a converged solution are that all single field solutions are fulfilling the equilibrium equations. In addition, the interface of the coupled problem also has to be taken into account. This means that the external aerodynamic forces has to be balanced with the internal structural forces. As in every coupling step convergence on the structural field has to be granted, the FSI simulation reaches the equilibrium state when the interface force on CSM as well as on CSM side reach the same value.

To perform the numerical simulation, the whole FSI coupling environment is implemented in the institutes own research program CEAS++. Main program features are data mapping, data interpolation, data management as well as the customized external solver control units.

### 2.4 Aircraft Trim Algorithm

To evaluate the structural loading, the aircraft is trimmed with a given load factor in a quasi-steady flight condition. If no detailed lift slope is available or the structural sizing process causes a change in the stiffness of the wing, the aircrafts trim equations have to be solved within the FSI simulation run. In the trimmed flight configuration, the resulting forces and moments about the center of gravity are balanced. Therefore, trim variables like global angle of attack or flap deflections are used and defined in the trim vector $\overline{x}$. The non-balanced equilibrium residuals are expressed by the vector equation (9) and have to be zero in a successfully trimmed flight state.

$$R(\overline{x}) = 0 \tag{9}$$

Due to the aerodynamic and structural flexibility, the force or moment response $R(\overline{x})$ is non-linear in general. Hence, an iterative method is used to find $\overline{x}_{trimmed}$. The damped Newton method as defined in equation (10) is for this purpose used.

$$\overline{x}_{n+1} = \overline{x}_n - \lambda\left[H\left(R(\overline{x}_n)\right)\right]^{-1} \nabla \mathrm{R}(\overline{x}_n) \tag{10}$$

In principal, the used method can be characterized by minimizing $\mathrm{R}(\overline{x}_n)$. The necessary gradients to approximate the inverse Hessian matrix are determined by first order finite difference scheme. Solving the trim equation is stopped, when a predefined convergence value is reached. Within the extra sub-iterations for the trim algorithm, the aircraft is treated as a rigid body aircraft in the current flexible deformed but not converged state. Thus, the simulation is separated in an inner-loop, where the FSI problem solves the elastic aircraft problem and in an additional outer-loop, for solving the trim equation on a quasi-rigid configuration as shown in Figure 2. The simulation is finished, when the inner- and outer-loop iterations are converged.

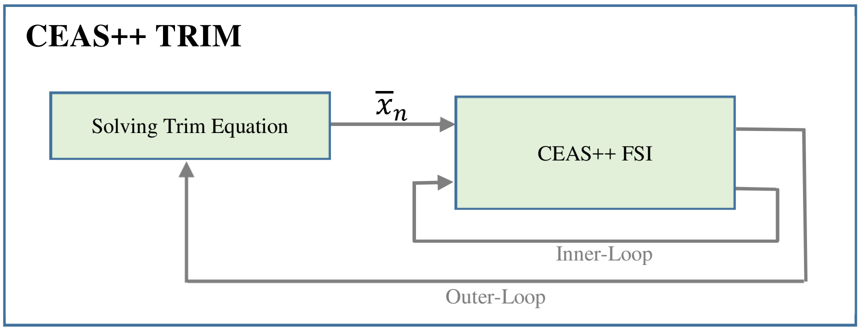


Figure 2: CEAS++ Trim procedure

## 3 COMPUTATIONAL MODELS FOR FLEXIBLE WING CASE STUDY SIMULATION

To investigate the influence of a high AR flexible wing on full aircraft level, a generic transport aircraft with basic wing plan form parameters as presented in Figure 3 is used. The used case study is a dragon configuration with a MTOW of 95t and is generated to investigate structural design solutions which are going along with a high AR composite wing.

| Wing Area (S) | Aspect Ratio (AR) | Taper Ratio (TR) | Leading Edge Sweep |
|---|---|---|---|
| 158 m² | 14.0 | 0.2 | 25° |

Table 1: Wing planform parameters

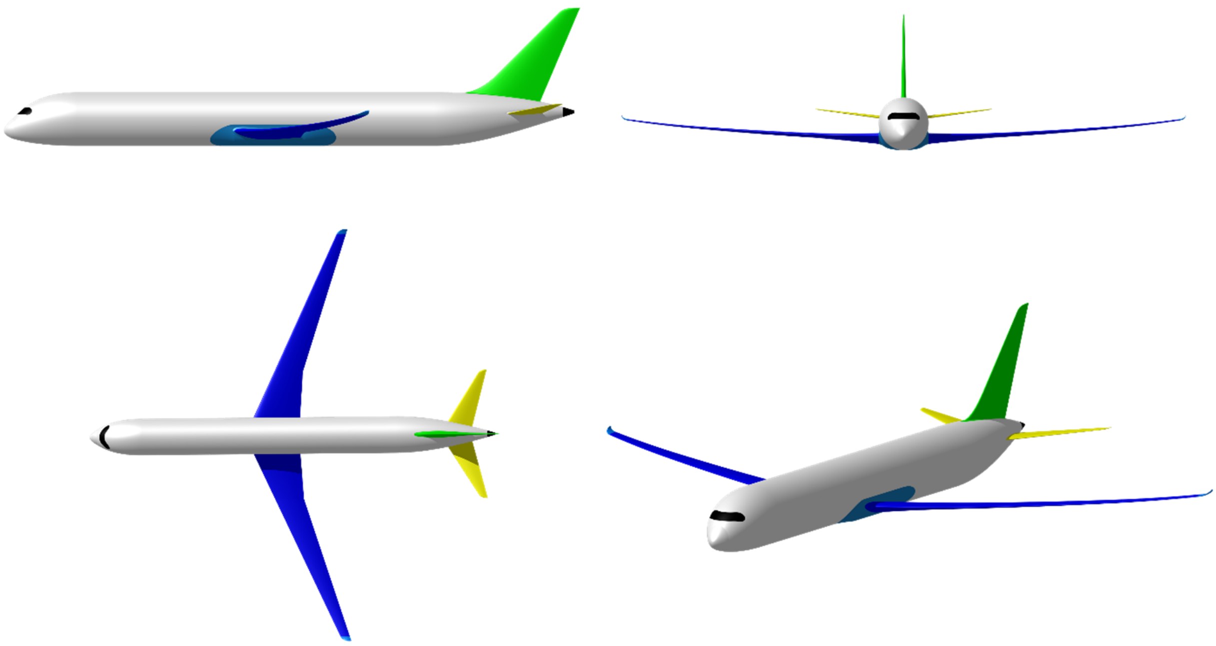

Figure 3: Flexible wing aircraft configuration

The presented work focuses on the development of the flexible wing, which is shown in Figure 4. The structural design is considering the intensive use of modern composites materials. Therefore, for the skin and main load carrying components like ribs, stringers and spars, monolithic CFRP layups are used. The leading and trailing edge devices are designed as sandwich structures for a very light weight structural design.
The wing has four leading edge devices, an inner and outer flap for high lift, one high speed aileron located near the wing kink and an additional outer aileron for lower flight speeds. The wing box, center wing box included, consist of 30 ribs between front and rear spar. To support the skin especially against elasto-stability failure, additional structural stiffness is introduced by Ω-stringers in wing span direction.

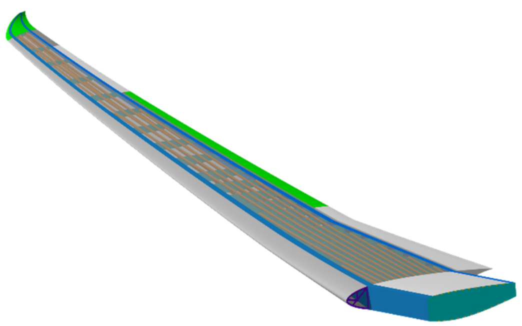

Figure 4: Flexible Aircraft Wing Structural Design

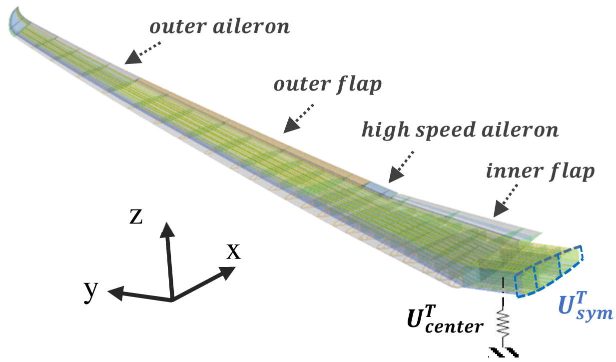


Figure 5: Finite Element Model and related support boundary condition

### 3.1 Finite Element Wing Model

The wing deformation in respect to the applied load is solved by a computational structural mechanics (CSM) model. As structural discretization, the Finite Element Method (FEM) with shell elements is used. For the different components with overlapping areas like skin to spar, the CFRP layup is defined in a smeared stiffness approach. Due to its dimensions the used model has the advantage of a highly accurate stiffness representation of all interacting structural components with low computational effort. The anisotropic behavior is represented by the classical laminate theory. The connection of the flaps to the wing box is defined in a way that no artificial stiffening occurs by detaching the skin edges. The applied aerodynamic loading is only transferred via the flap ribs into the rear spar hinge connecting points.

For the presented work only symmetric flight maneuvers are considered and therefore only a half model is used. At the symmetry plane, as shown in Figure 5, symmetric boundary conditions $U_{sym}$ are applied. To present a free flying wing, an additional modified boundary condition $U_{center}$ for the translation direction in x and z as well as rotational degree in y has to be realized. As a non-constrained model is not valid for static simulations, the wing will be clamped with an additional spring support. By this boundary condition, the system of equations gets closed and can be solved. In addition, the spring compensates the unbalanced forces in the trim calculation. In other words, if the aircraft is in a trimmed flight configuration, the resulting force and therefore the spring displacement is zero.

$$\boldsymbol{U}^{\boldsymbol{T}}_{\boldsymbol{sym}} = [X \quad 0 \quad Z \quad 0 \quad Y_{rot} \quad 0] \tag{11}$$

$$\boldsymbol{U}^{\boldsymbol{T}}_{\boldsymbol{center}} = \begin{bmatrix} 0 & Y & (Z_{support} = 0) & X_{rot} & 0 & Z_{rot} \end{bmatrix} \tag{12}$$

### 3.2 Aerodynamic Wing Model

The aerodynamic forces are calculated by Computational Fluid Dynamic (CFD) methods, solving the steady compressible Reynolds Average Navier Stokes (RANS) equations. A Finite Volume pressure based solver is used for this purpose. As turbulence model, the eddy viscosity based $k - \omega$ modified Shear Stress Transport model with additional wall function correction is used. The resolution of the flow field discretization is a compromise between the computational effort and physical reasonable results.

The flow domain as presented in Figure 6 to Figure 8 is discretized with hex dominated cells. Higher cell density is chosen in the near field close to wing to cover important flow effects next to the wing. Because the aerodynamic model is later coupled with the CSM model, covering normal forces is most important while keeping the computational effort as low as possible. Due to this compromise, the number of cells in the trade-off study is set to be around 12.0 Mio. Especially in the case when an evaluation of aerodynamic efficiency, hence drag is in focus, the aerodynamic grid has to fulfill much higher accuracy requirements.

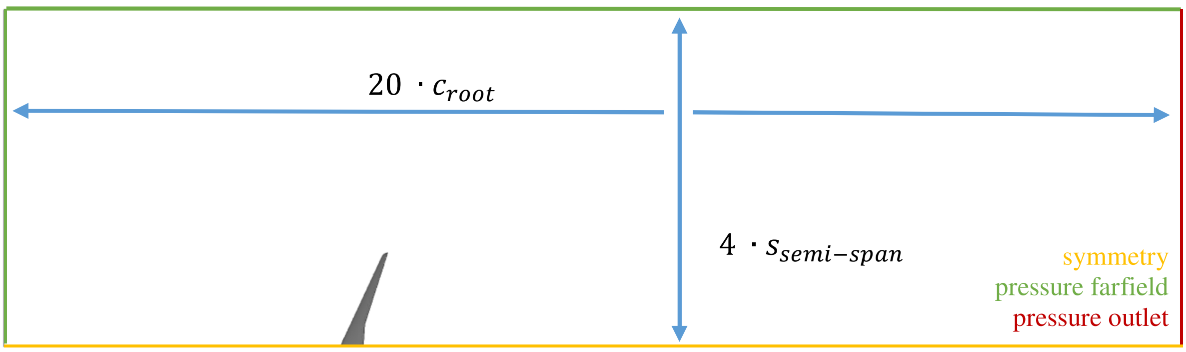


Figure 6: CFD domain top-view

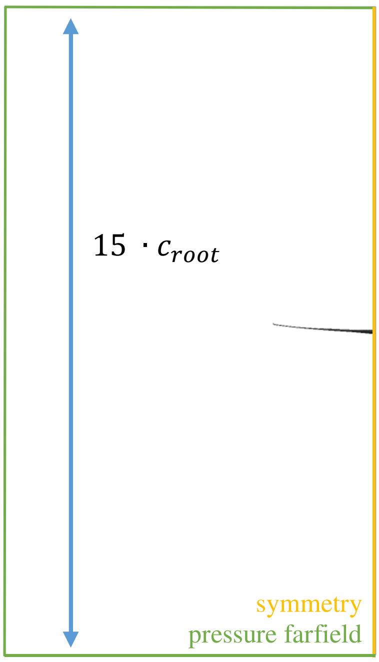


Figure 7: CFD domain front-view

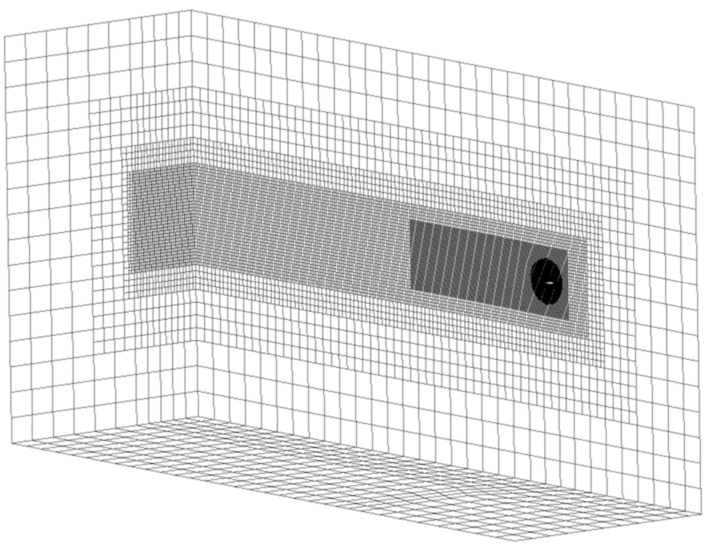

Figure 8: Hex cell discretized CFD domain

### 3.3 Initial Structural Sizing and Mesh Morphing Test

The FSI simulations are computationally expensive. That is why the implemented models have to pass basic initial tests, which could otherwise cause difficulties in the later coupled simulation.

As non-linear simulations are performed on the structural side, the wing has to be already pre-sized in a way that no elasto-static instabilities, like buckling, occur. The resulting aerodynamic forces from a reference rigid case are used to perform a linear buckling analysis. Basically it would also be possible to perform a structural sizing optimization at this point. Choosing the right pre-sizing load is essential and not that straight forward. In a first simple run, the highest angle of attack (AoA) of the full aircraft has the highest wing root load condition, but is not necessarily the most critical case in the fully coupled simulation. Due to the wings flexibility and the sweep, most of the lift is produced at the wings root at high AoA. The critical buckling case occurs at moderate AoAs, when the wing is loaded higher at the outer wing parts.

On CFD side, the domain mesh morphing stability has to be proven. During the trim calculation, the wing can undergo large deformations. The CFD grid and the used morphing method has to be stable enough in order not to produce bad quality cells, which would lower the simulation convergence. In the worst case, the morphing procedure would generate folded mesh cells and cause an error. The FSI run will fail. To avoid this a fast mesh morphing run with a representative displacement boundary condition is performed at the beginning. This should be as similar as possible to the expected wing deformation. A linear combination of the natural eigenvectors of the wing is used as a test case. First wing bending and torsion-bending dominated modes as shown in Figure 9 and Figure 10 are therefore good choices. The superposition of the modes is scaled and applied to the wing morphing until the mesh quality criteria fail. The results are used to adapt the grid or morphing algorithm until it fulfils the required boundary conditions.

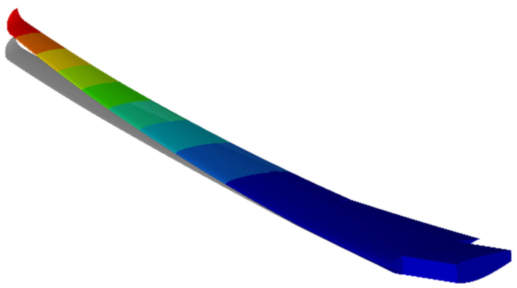

Figure 9: 1st wing bending eigenmode

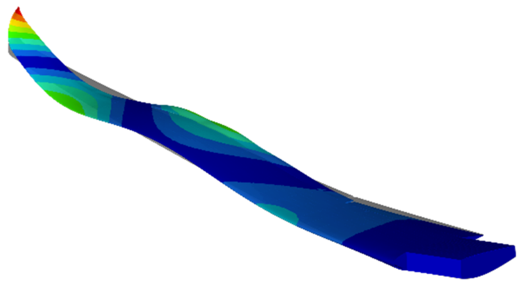

Figure 10: Torsion-3rd-Bending dominated eigenmode

With the available displacement field and corresponding pressure force field, the final mapping between CSM and CFD can be evaluated. Therefore, the interface work on CSM and CFD side is evaluated.

$$\sum_i \bar{F}_i \cdot \bar{U}_i = W_{interface} \tag{13}$$

For the presented wing a total error between both sides of -0.015% is identified. These errors are occurring due to different mesh resolutions around the leading edge, especial at the wing tip. For the further progress these errors are acceptable.

## 4 FLEXIBLE WING FSI CASE STUDY

In the first simulation case, the flexible wing is clamped to study the different behaviors of linear and non-linear flexible wing compared to a rigid wing. In this case, linear and non-linear simulation is related to the structural field. These results are further used as reference control values for the trim algorithm. As reference flight condition, an altitude of $4500m$ at a speed of $Ma = 0.54$ is used. The flight state is typical for end of approach and start of climbing. The lift force vs. the aircraft AoA is shown in Figure 11. Compared to the rigid wing, both linear and non-linear structural behavior showing the typical lift reduction at higher load cases due to the wing washout. Differences in total lift forces between linear and non-linear treatment can be found only in higher load cases. For the given wing structure, and as long as no flaps are used, the assumption of a linear structure is justified. In case of flaps included, the non-linearities due to large rotations are not negligible anymore.

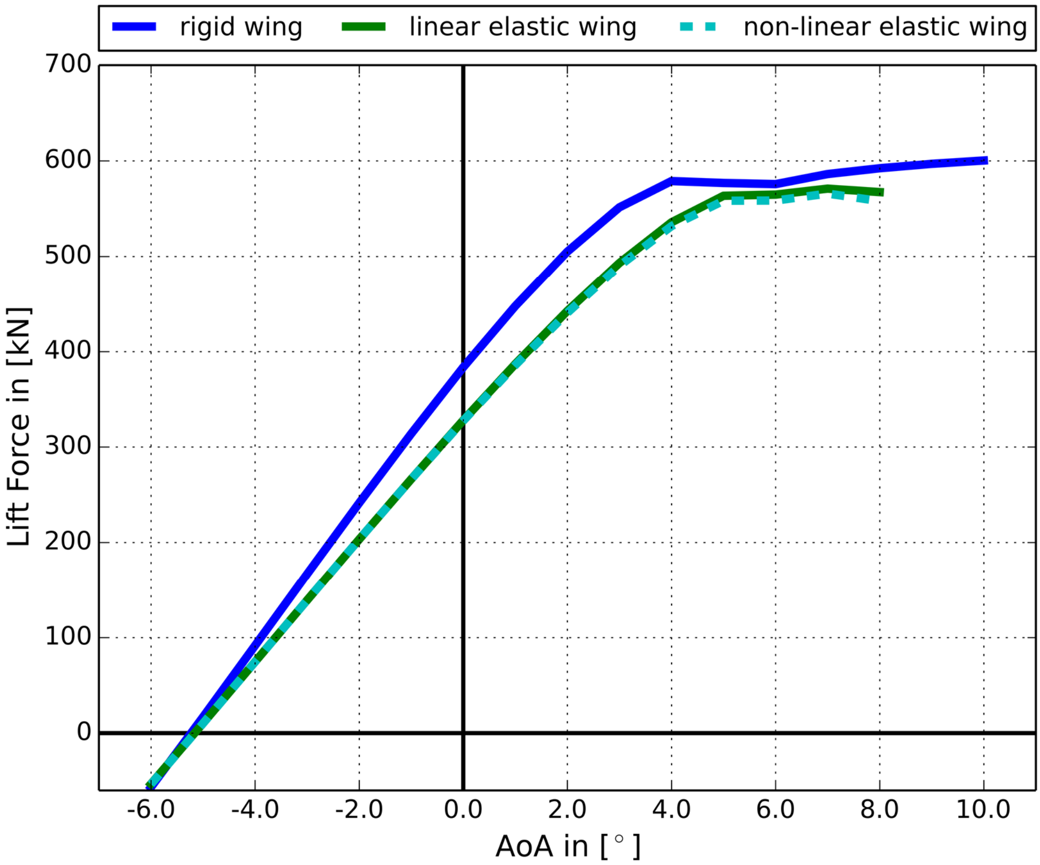


Figure 11: Lift vs. Angel of Attack (AoA)

### 4.1 Trim Calculation

In the presented case, it is assumed that the aircraft pitch angle is zero and the elevator flaps ideally balance the pitch moment. Hence, the trim equation as described in chapter 2.4 can be simplified as in equation (14) with the trim-variable $\alpha$, the aircraft weight G and vertical lift component $L_z$. The percentage on lift produced by the empennage and fuselage are not considered.

$$R(\alpha) = \frac{G}{2} - L_z(\alpha) \tag{14}$$

The results of the outer-loop iterations for different load factors $n_z$ are plotted together with the lift slopes as reference in the following Figure 12 to Figure 15. The trim iteration is starting at a global AoA of $\alpha = 0.0°$. The outer-loop iteration is updated at every third inner-loop with an under relaxation of $\lambda = 0.9$. The first simulation outcome showed, that the calculation of the trim-variable gradients with a rigid body wing overestimates the value for $\alpha_{n+1}$ especially at the first outer-loop iteration. This problem can be solved by stabilizing the solver with a $\alpha$ gradient limiting factor. With the final damping and stability parameters, a smooth and fast convergence to the equilibrium state for different load factors could be achieved.

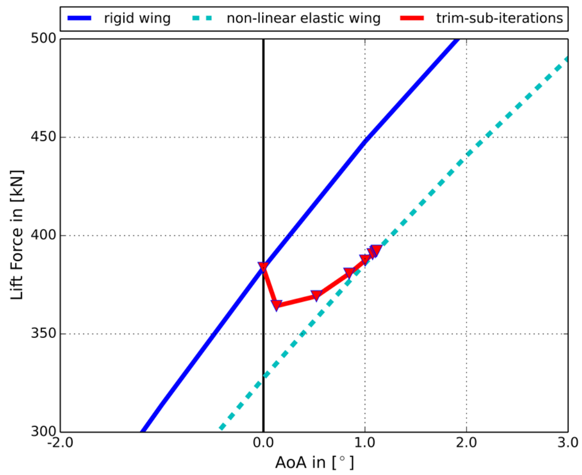


Figure 12: Trim Calculation $n_z = 1.0$

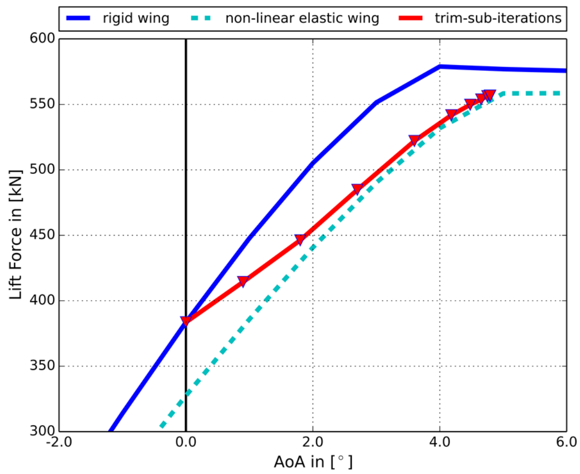


Figure 13: Trim Calculation $n_z = 1.425$

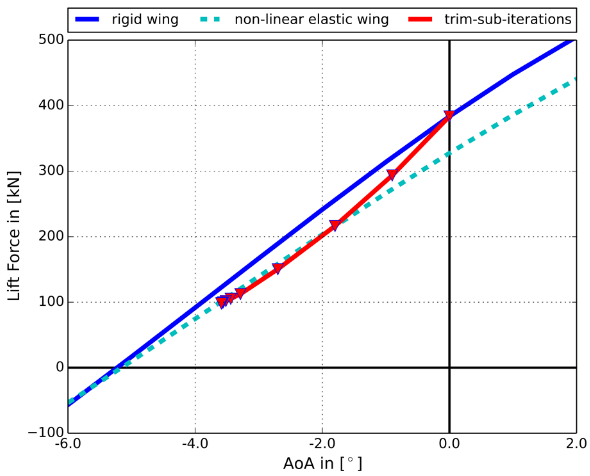


Figure 14: Trim Calculation $n_z = 0.25$

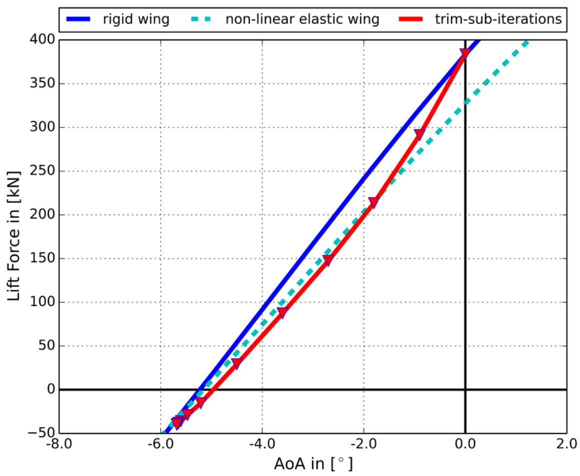


Figure 15: Trim Calculation $n_z = -0.1$

Convergence of the trim equation is proven by evaluating the change of the trim variable and the residual forces on the trim-support boundary condition. For the different load conditions these are shown in Figure 16 and Figure 17.

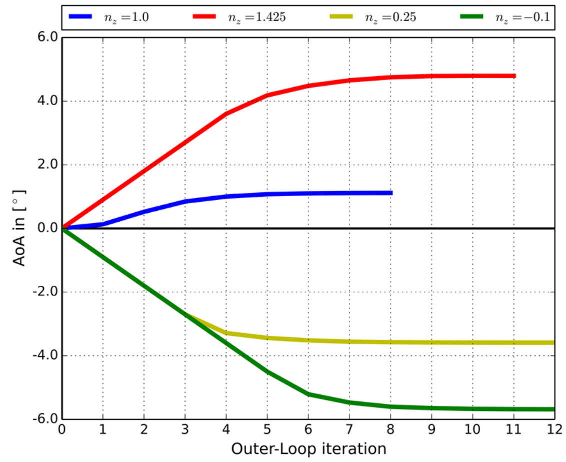


Figure 16: AoA convergence value

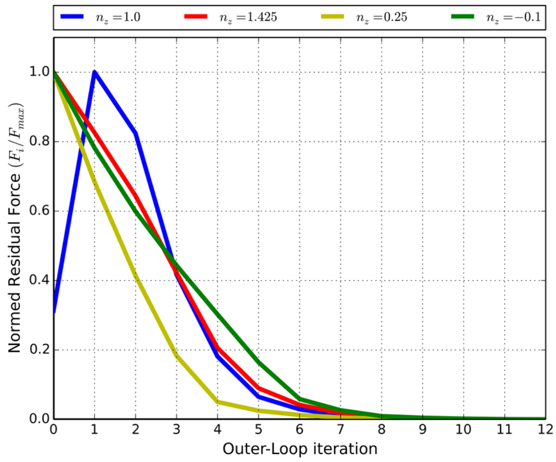


Figure 17: Force Residuum value

## 4.2 Non-Linearity Effects at Higher AoA

As outlined in the introduction, the presented work aims to introduce high fidelity methods in the aircraft design process with respect to the structural design and aeroelasticity task. In Figure 18 the results of the lift distribution are presented for an AoA of 4° and 8° for both the rigid and the elastic wing. Comparing the two rigid structure solutions, one can see that the lift abruptly decreases around 38% of the semi-wing span. The initial wing plan form as well as the aerofoil incidence was designed with a potential based aerodynamic model, with poor boundary layer models. Eventual flow separation cannot be treated with adequate accuracy at an AoA of 8°. The flow field as shown in Figure 19 verifies that the break-down in lift is caused by a detached flow.

Compared to an AoA of 4°, more lift is produced near the wing root. This is a favorable solution, as the root bending moment is reduced. In case of a buckling evaluation it has to be considered, that the higher AoA ranges are not necessarily the main design driver. For the maximum root bending moment this might be true as shown in Figure 20. As the acting lift at lower AoA is located at the outer wing and the skin laminate thickness is reduced due to mass reduction, the critical location for the presented wing could be identified at around 35% of the semi-wing span at $Ma = 0.54$ and $AoA = 4°$.

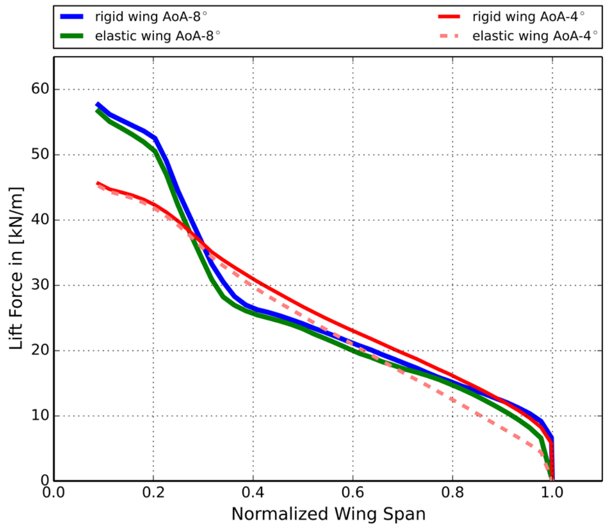


Figure 18: Lift distribution along the normalized semi-wing span

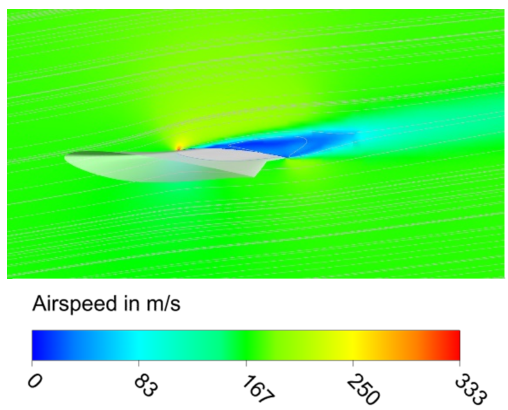


Figure 19: Detached flow at 38% semi-wing span at $Ma = 0.54$ and AoA = 8°

Comparing the lift distribution in Figure 18 for a rigid and elastic wing at AoA of 4°, one can figure out, that especially in the outer wing section the lift for a constant AoA is decreased. This is caused by the wing washout effect due to the wing's sweep of 25° and wing bending. This is a major non-linear influence of the coupled FSI system. Especially with increasing wing flexibility and higher AR, this effect will be much more distinctive. In the presented case, it is even that way, that around 5° AoA the wing washout is compensating most of the additional lift, so that the lift in the outer wing section will stay nearly constant. This is indicated by the different lift distributions depicted in Figure 22. A further side effect is, that the wing root bending moment is also nearly constant. Considering now both effects, flow separation and wing washout together shows how non-linearities can take an important role. Especially when the local AoA is decreased in the outer wing section. The change in total lift production is produced by the inner wing alone. On the other hand, the local root airfoil has a relatively high thickness, so that no flow separation occurs. Due to the high root bending moment, the inner wing section is quite stiff, so elasticity effects play a minor role.

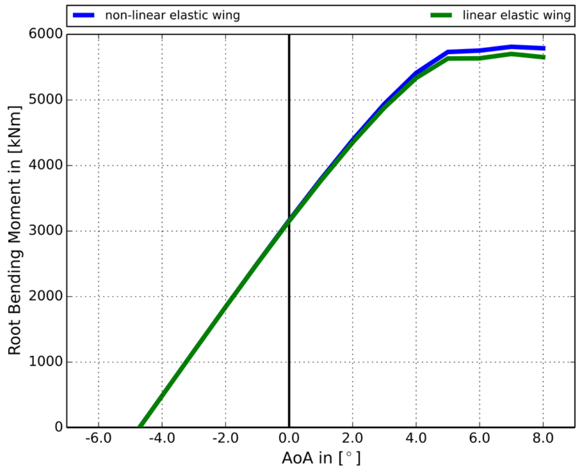


Figure 20: Root-Bending moment for different AoA

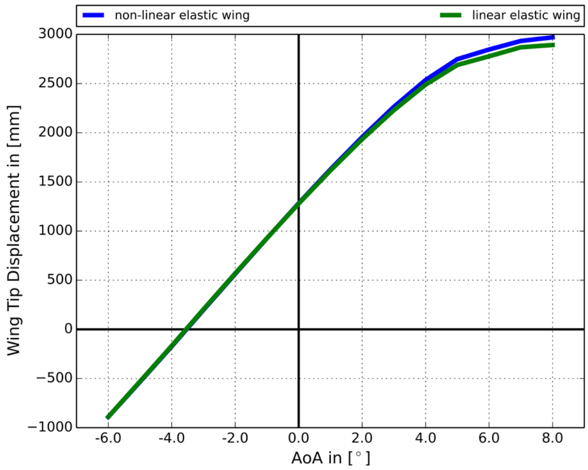


Figure 21: Wing tip deflection for different AoA

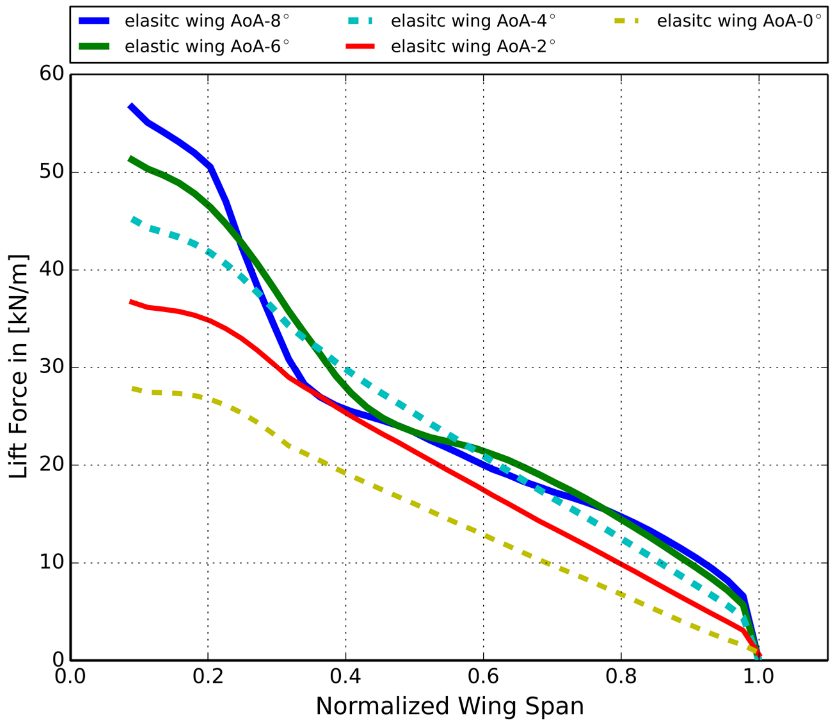


Figure 22: Lift distribution along the normalized semi-wing span for different AoA

For a final evaluation of the flexible wing, it is necessary that configurations with the same load factor and thus the same total lift are compared. The trim algorithm is used to bring the aircraft to an equilibrium state. The aircrafts global AoA results for two load conditions $n_z = 1.0$ and $n_z = 1.4$ as depicted in Table 2.

| | |
|---|---|
| $n_z = 1.0$ - rigid | $\alpha = 0.13°$ |
| $n_z = 1.0$ - elastic | $\alpha = 1.12°$ |
| $n_z = 1.4$ - rigid | $\alpha = 2.95°$ |
| $n_z = 1.4$ - elastic | $\alpha = 4.42°$ |

Table 2: Trim Variable Values

Due to the wings washout, for both cases the wing lift is reduced in the outer wing section. To compensate the loss in lift, the global AoA has to be increased. The resulting lift is shifted closer to the wing root for both cases. From a structural load point of view, this characteristic is favored. Drawbacks can be identified by looking at the aerodynamic drag as shown in Figure 24. Due to the higher AoA for $n_{z,rigid} = 1.0$ to $n_{z,elastic} = 1.0$ the drag is increasing from 19.2 $kN$ to 20.4 $kN$ and for $n_z = 1.4$ from 35.1 $kN$ to 43.4 $kN$. So the increasing drag would have to be balanced through a lighter structure. In general, the positive effects are dominating and the drawbacks can be further reduced by an improved design with methods as presented.

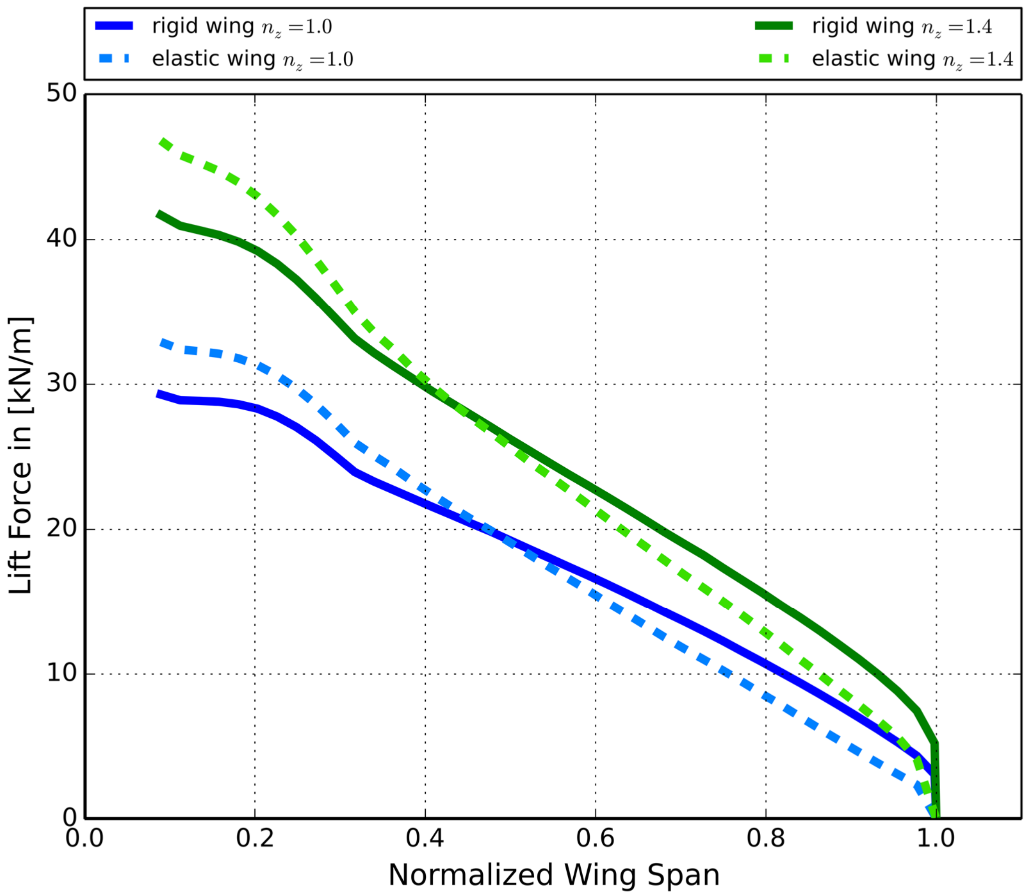


Figure 23: Lift distribution rigid vs. elastic trimmed aircraft

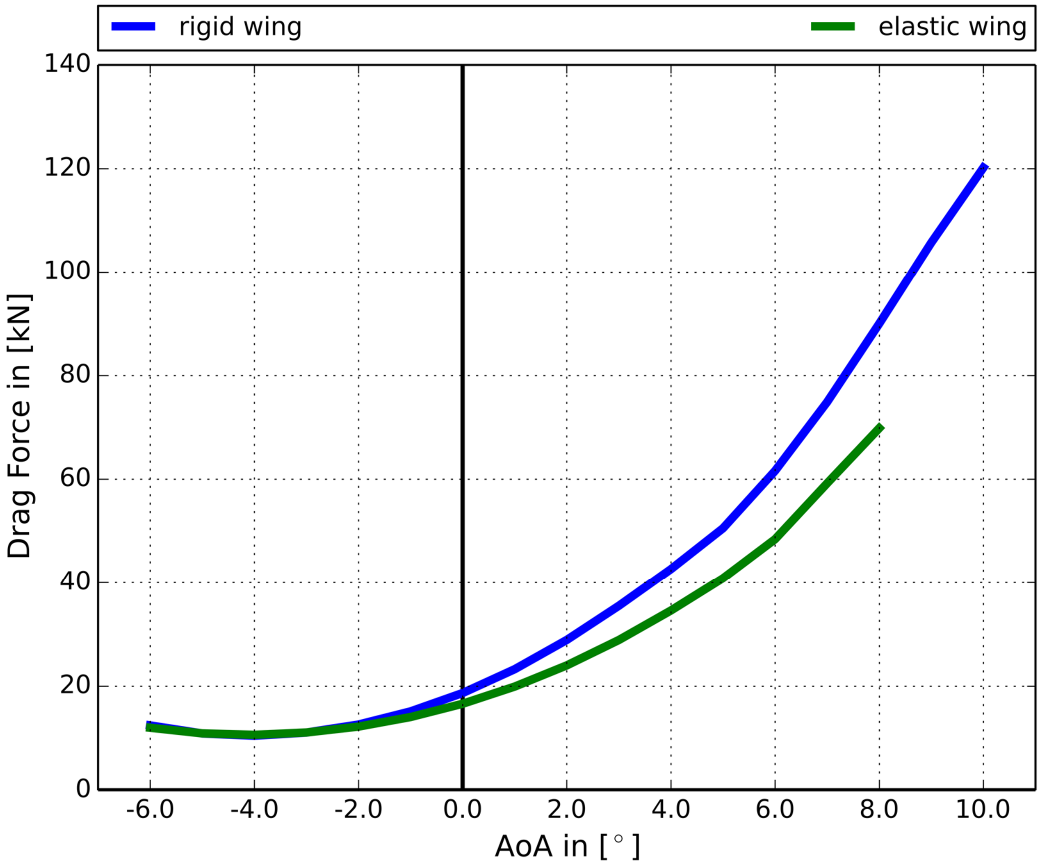


Figure 24: Drag vs. AoA

## 5 REVIEW AND OUTLOOK

In the presented paper, a method for high fidelity trim calculation of a high aspect ratio wing for a transport aircraft under aero-elastic conditions is presented. Different non-linear effects of the overall aircraft are depicted and the demand for high fidelity simulations in early conceptual design are discussed. Special requirements for structural aircraft design are reconsidered and demonstrated on two different quasi-steady aircraft load cases.

The focus of the presented work is oriented on the computational methods. The wing and aircraft configuration is chosen as a possible application for novel aircraft demonstrations. For the wing, four structural sizing zones are defined and a preliminary component sizing is done via engineering knowledge. In the next step, more sizing zones and optimization tools are applied. This will enable the possibility to further reduce the structural weight and enable a further increase in wing flexibility. With increasing wing flexibility, the methods become more expressive, since the rigid, linear and non-linear solutions will differ more substantially.

On the computational side, the elevator is included to trim the pitch moment. For this, robust sliding mesh technics have to be established to handle the gaps between empennage and flap. It is expected, that with an increasing number of trim variables the computational effort for the trim gradients is excessively increasing. Therefore, further non-linear solution methods to solve the trim equation based on approximation methods of the Hessian matrix are proven.

## 6 REFERENCES

[1] Farhat C., Lesoinne M., LeTallec P. (1998). *Load and Motion Transfer Algorithms for Fluid/Structure Interaction Problems with Non-Matching Discrete Interface: Momentum and Energy Conservation, Optimal Discretization and Application to Aeroelasticity*. Computer Methods and Applied Mechanical Engineering, Vol. 157 No. 1.

[2] Popp A. (2012). *Mortar Methods for Computational Contact Mechanics and General Interface Problems*. PhD. Thesis Technical University of Munich

[3] Breuer M., et al. (2012). *Fluid–structure interaction using a partitioned semi-implicit predictor–corrector coupling scheme for the application of large-eddy simulation*. Journal of Fluids and Structures.

## COPYRIGHT STATEMENT